Band Engineering in Core/Shell ZnTe/CdSe for Photovoltage and Efficiency Enhancement in Exciplex Quantum Dot Sensitized Solar Cells

Shuang Jiao,[†] Qing Shen,[‡,§] Iván Mora-Seró,[⊥] Jin Wang,[†] Zhenxiao Pan,[†] Ke Zhao,[†] Yuki Kuga,[‡] Xinhua Zhong,[*,†] and Juan Bisquert[⊥,∥]

[†]Key Laboratory for Advanced Materials, Institute of Applied Chemistry, East China University of Science and Technology, Shanghai 200237, China, [‡]Department of Engineering Science, University of Electro-Communications, 1-5-1 Chofugaoka, Chofu, Tokyo 182-8585, Japan, [§]CREST, Japan Science and Technology Agency (JST), 4-1-8 Honcho, Kawaguchi, Saitama 332-0012, Japan, [⊥]Photovoltaic and Optoelectronic Devices Group, Department de Física, Universitat Jaume I, 12071 Castelló, Spain, and [∥]Department of Chemistry, Faculty of Science, King Abdulaziz University, Jeddah 21589, Saudi Arabia

ABSTRACT Even though previously reported CdTe/CdSe type-II core/shell QD sensitizers possess intrinsic superior optoelectronic properties (such as wide absorption range, fast charge separation, and slow charge recombination) in serving as light absorbers, the efficiency of the resultant solar cell is still limited by the relatively low photovoltage. To further enhance photovoltage and cell efficiency accordingly, ZnTe/CdSe type-II core/shell QDs with much larger conduction band (CB) offset in comparison with that of CdTe/CdSe (1.22 eV vs 0.27 eV) are adopted as sensitizers in the construction of quantum dot sensitized solar cells (QDSCs). The augment of band offset produces an increase of the charge accumulation across the QD/TiO_2 interface under illumination and induces stronger dipole effects, therefore bringing forward an upward shift of the TiO_2 CB edge after sensitization and resulting in enhancement of the photovoltage of the resultant cell devices. The variation of relative chemical capacitance, C_μ, between ZnTe/CdSe and reference CdTe/CdSe cells extracted from impedance spectroscopy (IS) characterization under dark and illumination conditions clearly demonstrates that, under light irradiation conditions, the sensitization of ZnTe/CdSe QDs upshifts the CB edge of TiO_2 by the level of ~50 mV related to that in the reference cell and results in the enhancement of V_{oc} of the corresponding cell devices. In addition, charge extraction measurements have also confirmed the photovoltage enhancement in the ZnTe/CdSe cell related to reference CdTe/CdSe cell. Furthermore, transient grating (TG) measurements have revealed a faster electron injection rate for the ZnTe/CdSe-based QDSCs in comparison with the CdSe cells. The resultant ZnTe/CdSe QD-based QDSCs exhibit a champion power conversion efficiency of 7.17% and a certified efficiency of 6.82% under AM 1.5G full one sun illumination, which is, as far as we know, one of the highest efficiencies for liquid-junction QDSCs.

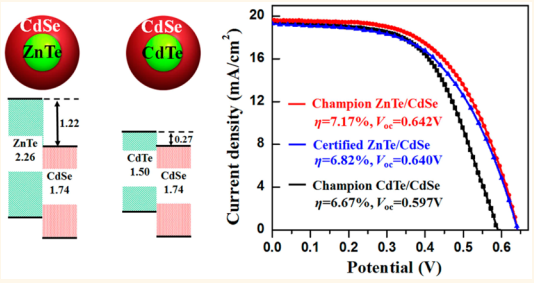

KEYWORDS: quantum dot sensitized solar cells · high photovoltage and efficiency · band gap engineering · type-II core/shell structure · ZnTe/CdSe quantum dots

Quantum dot sensitized solar cells (QDSCs) are attracting increasing interest as a promising low-cost candidate for third-generation solar cells because of the various advantages of QD sensitizers and the potential possibility of multiple exciton generation (MEG).[1−6] Despite continuous progress in the last years, the potential power of QDSCs is overshadowed by their moderate performance with a reported highest power conversion efficiency (PCE) of 5−7%.[7−14] The reasons for the relatively low PCE of QDSCs are associated in part with the nature of QD sensitizers used.[15−23] Ideal QD sensitizers should bear the characteristic of wide absorption range, high conduction band (CB) edge, and free of trap-state defects.[15,16] Among the exploited QDs, type-II core/shell QDs, which are composed of core-localizing holes and shell-localizing electrons, have shown great promise in serving as sensitizers in QDSCs.[8,24−31] The spatial separation of electron and hole in type-II core/shell QDs enables an enhanced electron injection rate and retards the charge recombination

* Address correspondence to zhongxh@ecust.edu.cn.

Received for review November 20, 2014 and accepted January 6, 2015.

Published online January 06, 2015
10.1021/nn506638n

process because the shell can act as a tunneling barrier for the hole localized in the core.[28,29] Furthermore, the long-lived charge separation in type-II QD under illumination can create a dipole moment *via* the accumulation of negative charges in TiO_2 substrate/electron conductor and positive ones in the cores of the type-II QDs. The created dipole moment upshifts the TiO_2 CB edge and brings forward higher open photovoltage of the resultant cell device.[32,33] In addition, due to the "spatially indirect" energy gap, or exciplex state, expanded light-absorption is observed in type-II QDs, producing an increase of photocurrent in the corresponding solar cells.[8,24] Despite the efficiency improvement registered with previously reported CdTe/CdSe type-II core/shell QDs, the resultant efficiency is still limited mainly due to the relatively low open circuit potential (V_{oc}).[8] Thus, an increase of V_{oc} is mandatory for further optimization of QDSCs performance.

In serving as light-absorber, ZnTe/CdSe type-II core/shell QD is potentially more advantageous over CdTe/CdSe because the former shows much larger CB offset compared to that of the latter (1.22 eV vs 0.27 eV) as illustrated in Figure 1.[8,34] The augmentation of band offset produces an increase of charge accumulation at the interface of QD/TiO_2 under illumination inducing stronger dipole effects and therefore brings forward a greater upward shift of the TiO_2 CB edge after sensitization and results in enhancement in photovoltage of the resultant cell devices.[32,33] Herein, high-quality ZnTe/CdSe core/shell QDs with near-infrared absorption edge were adopted as sensitizers in the construction of QDSCs for the first time. The resultant ZnTe/CdSe QDSCs exhibit a champion PCE of 7.17% and a certified efficiency of 6.82% under AM 1.5G full one sun illumination, which is, as far as we know, the highest efficiency for liquid-junction QDSCs.[7−10,35] The increase of PCE is mainly derived from the enhancement of photovoltage through the band engineering of type-II core/shell QDs, which produces an upward shift of the TiO_2 CB edge after sensitization under illumination. This assumption has been confirmed by the impedance spectroscopy (IS) characterization under dark and illumination conditions and also by the charge extraction measurements.

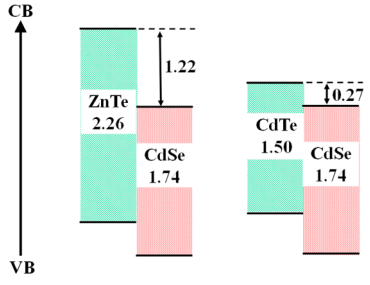

Figure 1. Schematic diagram of the band gap and band offsets (in eV) for the interfaces between bulk ZnTe/CdSe and CdTe/CdSe.

RESULTS AND DISCUSSION

Optoelectronic Properties. ZnTe/CdSe core/shell QDs (5.3 nm) with an absorption onset wavelength of ~850 nm developing from a 3.2 nm ZnTe core and 2.1 nm CdSe shell were synthesized according to the literature method,[36] and the detailed synthetic procedure and optical characterization are available in the Supporting Information. The photovoltaic performance of this sized ZnTe/CdSe QDs was proven to be the best one in our experimental results; therefore, only this size of QDs will be considered hereafter. For comparison, identical sized (5.3 nm) CdSe QDs with absorption onset wavelength at 650 nm (Figure S2, Supporting Information)[37] and the previously reported CdTe/CdSe type-II core/shell QDs containing a 2.7 nm CdTe core and a 2.2 nm thickness CdSe shell with absorption onset wavelength at ~850 nm (Figure S3, Supporting Information) were also synthesized and used as sensitizers in the construction of reference solar cells.[8] Because of their chemical instability, ZnTe QD based solar cells were not investigated.

Deposition QDs onto TiO_2 Electrodes. Following our previous reports,[7−9,37,38] the initial oil-soluble ZnTe/CdSe, CdTe/CdSe, and CdSe QDs were transferred into MPA-capped water-soluble QDs *via* ligand exchange. The sensitization of photoanodes with high QD loading and uniform distribution of QD sensitizers was achieved through the self-assembly of MPA-capped QDs by pipetting the MPA-QD aqueous dispersions on TiO_2 film and allowing them to remain at ambient atmosphere for 2−4 h.[7−9,37,38] Figure 2a shows the absorption spectra of ZnTe/CdSe, and reference CdTe/CdSe, CdSe QDs sensitized TiO_2 films with only 6.0 μm transparent layer. It was found that the sensitized photoanode films show absorption characteristics similar to those of their corresponding dispersions in solvents. This indicates that the particle size was not changed in the process of immobilization. From the wide-field TEM images of both plain and ZnTe/CdSe QD sensitized films (Figure 2b,c), we find that the surface of TiO_2 particles (with size of 20−40 nm) is covered densely by smaller dots (ZnTe/CdSe QDs with size ~5 nm). This gives qualitative information on the high coverage of QD on the surface of mesoporous TiO_2 film as confirmed also by the absorption spectra (Figure 2a).

Photovoltaic Performance. The solar cells were fabricated following standard literature methods. First, the QD sensitized TiO_2 photoanode films were further passivated by a thin layer of ZnS *via* dipping into Zn^{2+} and S^{2-} aqueous solutions alternatively for four cycles. Sandwich-type cells were constructed by assembling the sensitized photoanode and Cu_2S/brass foil counter electrode using binder clips and filled with polysulfide electrolyte (2.0 M Na_2S, 2.0 M S, and 0.2 M KCl aqueous solution). The current density (J)−photovoltage (V)

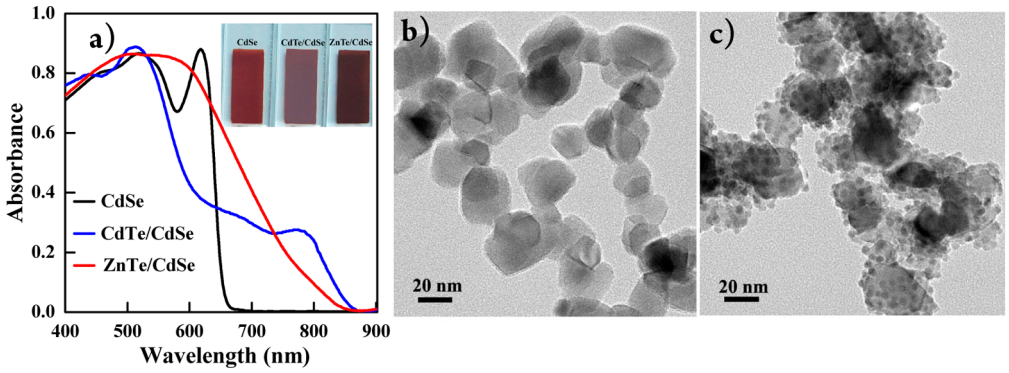

Figure 2. Optical spectral and TEM characterization of sensitized TiO_2 films. (a) Absorption spectra of ZnTe/CdSe, CdTe/CdSe, and CdSe QDs sensitized TiO_2 films with 6.0-μm transparent layer. Photographs of corresponding QD-sensitized TiO_2 film electrodes: wide-field TEM image of plain (b) and ZnTe/CdSe QD sensitized (c) TiO_2 films.

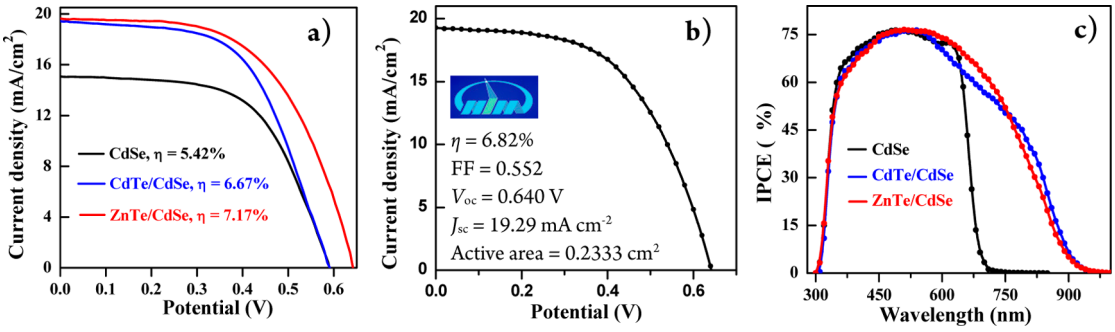

Figure 3. Photovoltaic performance of ZnTe/CdSe, and reference CdTe/CdSe and CdSe QDs based solar cells. (a) *J-V* curves of champion cells; (b) *J-V* curve of certified ZnTe/CdSe QDSCs; (c) IPCE curves.

curves of champion ZnTe/CdSe and reference CdTe/CdSe, CdSe cells with photoactive area of 0.233 cm^2 defined by masks under the irradiation of 1 full sun intensity (AM 1.5 G at 100 mW/cm^2) are shown in Figure 3a, and the average values for key photovoltaic parameters based on seven cell devices in parallel are listed in Table 1. The detailed *J*−*V* curves (Figure S4) and corresponding photovoltaic parameters (Table S1) for each cell are available in Supporting Information. It is noted that the photovoltaic performance of a representative ZnTe/CdSe cell was certified by the National Institute of Metrology (NIM) of China, and the certified PCE was 6.82% (Figure 3b, Table 1). The detailed information for this certification is available in the Supporting Information.

The obtained average PCEs are 6.89%, 6.46%, and 5.33% for ZnTe/CdSe, reference CdTe/CdSe, and CdSe cells, respectively. The champion ZnTe/CdSe cell exhibits the record PCE of 7.17% for liquid-junction QDSCs. It is noted that other types of quantum dot solar cells with more sophisticated configurations (such as depleted heterojunction solar cells) have yielded PCEs in the range of 7−9%.[35,39−41] In comparison, both the open-circuit voltage (V_{oc}, 0.646 V) and short-circuit current (J_{sc}, 19.35 mA/cm^2) for ZnTe/CdSe cells are remarkably greater than those from CdSe (0.595 V and 15.08 mA/cm^2, respectively). The higher J_{sc} for ZnTe/CdSe cells should be ascribed to the broader light-harvesting range of the ZnTe/CdSe sensitizer as well as to the higher electron injection rate as discussed below. It is interesting to compare the photovoltaic performances between the ZnTe/CdSe and CdTe/CdSe QDSCs, both of which belong to the exciplex QDSCs. ZnTe/CdSe QDSCs present better performance than CdTe/CdSe-based ones due to the higher V_{oc} in the former case. The intrinsic mechanism for the observed higher V_{oc} in ZnTe/CdSe QDSCs is discussed below.

TABLE 1. Photovoltaic Parameters Extracted from *J*−*V* Measurements

QDs	J_{sc} (mA · cm^{-2})	V_{oc} (V)	FF (%)	PCE (%)
ZnTe/CdSe[a]	19.65	0.642	0.57	7.17
ZnTe/CdSe[b]	19.29	0.640	0.55	6.82
ZnTe/CdSe[c]	19.35	0.646	0.55	6.89 ± 0.16
CdTe/CdSe[c]	18.53	0.597	0.58	6.46 ± 0.13
CdSe[c]	15.08	0.595	0.59	5.33 ± 0.07

[a] Performance of champion cell. [b] Certified performance. [c] Average values of seven cells in parallel.

The photocurrent response to incident light was evaluated by monochromatic incident photon to carrier conversion efficiency (IPCE) measurement. As shown in Figure 3c, the photocurrent response matches well the absorption profile with photocurrent onsets at wavelengths of 700 nm for CdSe and 900 nm for ZnTe/CdSe cells, respectively. IPCEs of ~75% in the

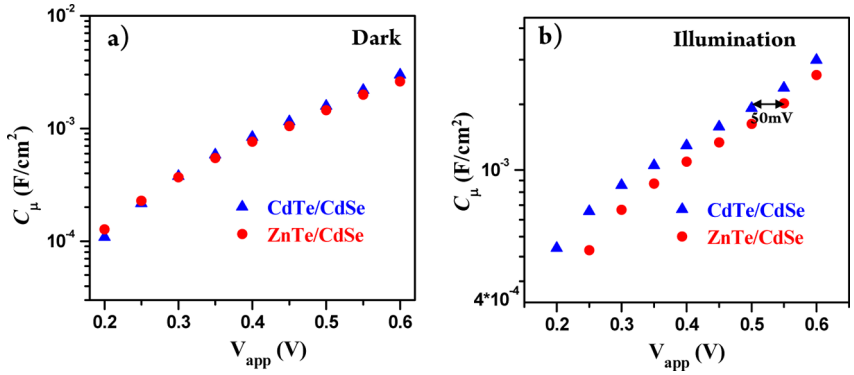

Figure 4. Dependence of chemical capacitance (C_μ) on applied voltage (V_{app}) extracted from EIS characterization of the QDSCs under dark (a) or illumination (b) conditions.

range of 360−680 nm were observed for CdSe and ZnTe/CdSe sensitizers, but a much broader response range (350−900 nm) was found for ZnTe/CdSe sensitizer in comparison with that for CdSe (350−680 nm). Similar IPCE was obtained for ZnTe/CdSe and CdTe/CdSe QDSCs, with nearly identical onset indicating analogous energy for the exciplex state. By integrating the product of incident photon flux density and cell's IPCE spectra, the calculated J_{sc} for ZnTe/CdSe, CdTe/CdSe, and CdSe based solar cells are 19.29, 18.24, and 14.51 mA·cm^{-2}, respectively, which are close to the measured values as shown in Table 1.

Impedance Spectroscopy. IS was employed to reveal the intrinsic mechanism of the V_{oc} enhancement in ZnTe/CdSe cells related to reference CdTe/CdSe cells since this technique can provide dynamic information about charge transport, accumulation, and recombination in cell devices. It is noted that EIS characterization was conducted under both dark and illumination conditions in order to verify the effect of TiO_2 CB edge upshift by ZnTe/CdSe sensitization under illumination related to that of CdTe/CdSe sensitization. Corresponding Nyquist curves for both cells under different bias are given in Figures S5 and S6 (Supporting Information). The chemical capacitance (C_μ), which reflects the capability of a system to accept or release additional carriers due to a change in the Fermi level and consequently reflect the density of states,[42] was extracted from the corresponding Nyquist curves with use of Z-view software under standard models.[17,42−44] From IS results (Figure 4a), we can find that under the dark conditions both ZnTe/CdSe and reference CdTe/CdSe cells have nearly identical C_μ values. This indicates that under dark conditions the two studied sensitizers exhibit similar impacts on the CB edge. This result is consistent with our previous reports.[7−9] Under the illumination conditions (Figure 4b), the C_μ values observed in ZnTe/CdSe cell are lower than those from reference CdTe/CdSe cells under the same potential bias. It is clearly seen that the photovoltage in the ZnTe/CdSe cell is ∼50 mV higher than that for the reference cell at the same C_μ values. This indicates that under light illumination conditions the sensitization of ZnTe/CdSe QD upshifts the CB edge of TiO_2 by the level of ∼50 mV related to that in the reference cell and results in the enhancement of V_{oc} in the corresponding cell devices. As similar recombination resistance has been observed for both samples, Figure S7 (Supporting Information); this shift of the CB is directly transferred to the $J-V$ curve. The observed value for the upshift of TiO_2 CB edge is in good agreement with the enhancement of V_{oc} for ZnTe/CdSe cell as observed in the $J-V$ measurement. This is reasonable since the V_{oc} value in a sensitized solar cell is determined by the TiO_2 Fermi level offset from the redox potential of the redox in electrolyte.[44,45] The observed upward shift of TiO_2 CB edge under the illumination of the type-II core/shell QD sensitized photoanode can be explained by the photoinduced dipole effect (PID) developed by Zaban and co-workers[32,33] where a capacitor-like device is created across the type-II core/shell QD sensitizers and TiO_2 matrix through the accumulation of negative charges in the TiO_2 and positive ones in the cores of type-II QDs. As a result, a relatively strong dipole is created, inducing an upshift of the TiO_2 CB edge and higher V_{oc} in the resultant cell devices. An appropriated, band engineering has allowed the enhancement of quantum confinement in the system of ZnTe/CdSe in comparison with CdTe/CdSe QDs and consequently a stronger dipole effect with the subsequent upward shift of TiO_2 CB edge. Moreover, the upward displacement of TiO_2 CB edge is obtained with no cost in the measured photocurrent.

Charge-Extraction Measurement. A charge-extraction measurement was employed to further verify the V_{oc} increase in ZnTe/CdSe cell related to reference CdTe/CdSe cell. The charge-extraction technique measures the accumulated charge at the photoanode as a function of V_{oc} values in the steady state under specific illumination. Figure 5 shows the dependence of accumulated charge density on steady-state V_{oc} created by the irradiation of different light intensities. Similar to the IS results, in this case a ∼50 mV higher photovoltage is also observed in the ZnTe/CdSe cell (Figure 5,

red circles) in comparison with that for the reference CdTe/CdSe cell (Figure 5, blue triangles) for the same charge density in the cells. This demonstrates clearly that there is ~50 mV upward shift of the CB edge of TiO_2 when the sensitizer is changed from CdTe/CdSe to ZnTe/CdSe QDs.

Transient Grating Measurement. The transient grating (TG) method is a pump−probe technique that can be used to study photoexcited carrier dynamics in semiconductor QDs by monitoring the time dependence of refractive index changes resulted from photoexcited carriers in the sample. The TG technique can be used to characterize carrier recombination, trapping, and electron transfer in QDSCs.[46−48] To study the excited-state dynamics of QD sensitizers and electron-injection rate from QDs to TiO_2 conductor as well as the effects of type-II core/shell structure, femtosecond (fs) TG setups were used to characterize the photoexcited carrier dynamics of ZnTe/CdSe and CdSe QDs deposited on insulating SiO_2 or TiO_2 films, and the corresponding results are shown in Figure 6. The detailed experimental set up of TG measurements is available in the Supporting Information. In the case of QDs on SiO_2 matrix, there is no electron transfer from QDs to SiO_2 due to the insulating character of SiO_2 substrate, while for QDs on TiO_2 matrix, photogenerated electrons in the QDs can inject into TiO_2. Thus, faster decay can be observed for both CdSe and ZnTe/CdSe QDs deposited on TiO_2 compared to those of QDs on SiO_2. Thus, by comparing the TG decay processes of the QDs on TiO_2 to those of QDs on SiO_2, the electron injection rate (k_{et}) from the QDs to TiO_2 can be calculated. Bi- or triexponential kinetic decays are found to be successful in fitting the TG response for QD deposited on SiO_2 or TiO_2 substrates, and the fitting parameters are listed in Table S2 (Supporting Information). Average decay times τ_{av} were calculated on the basis of these extracted values using the equation of $\tau_{av} = \Sigma_n(a_n\tau_n^2)/\Sigma_n(a_n\tau_n)$. It is noted that τ_{av} of ZnTe/CdSe QDs on SiO_2 is about 20 times larger than that of CdSe QDs on SiO_2. This result means that recombination of electrons and holes in ZnTe/CdSe core/shell QDs was much slower compared to that in CdSe QDs as expected above. Note that this recombination process is an internal recombination in the QD, different from the recombination of electrons in the TiO_2 analyzed by IS. Then, to see whether the electron injection rate (k_{et}) was affected by the core/shell structure or not, two kinds of electron injection rates based on average decay times τ_{av} and τ_1 were calculated using the equation of $k_{et} = 1/\tau_{TiO_2} - 1/\tau_{SiO_2}$. As shown in Table S2 (Supporting Information), k_{et} values from CdSe QDs to TiO_2 are 5.4×10^8 (based on τ_{av}) and 2.5×10^{10} s^{-1} (based on τ_1), while those from ZnTe/CdSe QDs to TiO_2 are 1.9×10^{10} (based on τ_{av}) and 5.2×10^{11} s^{-1} (based on τ_1), respectively. It is noted that the k_{et} value for CdSe QDs to TiO_2 observed in our case is at same level as obtained previously.[49] These results indicate that the ZnTe/CdSe core/shell QD structure can improve the electron-injection rate dramatically. This is due to the spatial separation of charge carriers in the ZnTe/CdSe type-II core/shell structure as observed in the previous case of the CdTe/CdSe system.[8] This favors electron injection into the oxide conductor despite the reduction of driving forces due to the upward shift of TiO_2 CB and brings forward the improved photovoltaic performance of the resultant solar cell devices.

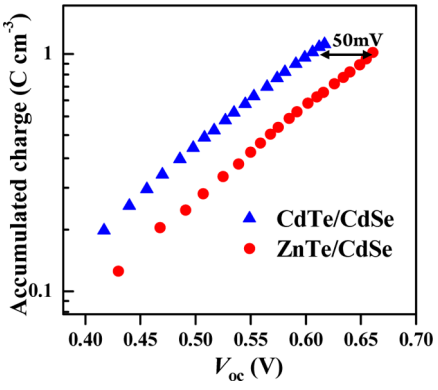

Figure 5. Accumulated charge density in photoanode against V_{oc}.

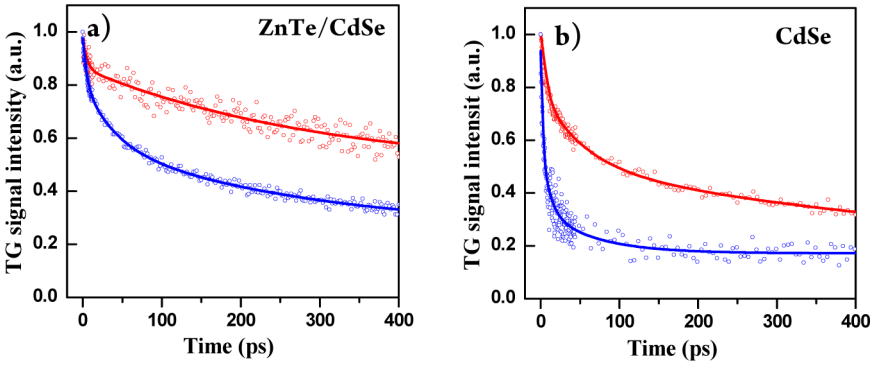

Figure 6. TG characterization on picosecond scale. Kinetic traces of the excitonic decay of ZnTe/CdSe QDs (a) and CdSe QDs (b) deposited on SiO_2 (red circles) and TiO_2 substrates (blue circles). The bold lines represent the corresponding multiexponential fit.

CONCLUSIONS

In summary, ZnTe/CdSe QDSCs with a record PCE of 7.17% and a certified PCE of 6.82% have been obtained. This result places the facile sensitized technology at the same level of conversion efficiency as with other sophisticated configuration quantum dot solar cells with more complicated manufacturing procedures. Accelerated electron injection and upshift of TiO_2 CB edge in the case of ZnTe/CdSe QDSCs with respect to reference CdSe and CdTe/CdSe cells have been confirmed by TG, IS, and charge-extraction characterizations, respectively. As sensitizers in QDSCs, type-II ZnTe/CdSe core/shell QDs are superior to plain CdSe QDs and possess the advantages of light harvesting range extending to the infrared spectral window and accelerated electron injection rate. Moreover, the increase of confinement with respect to CdTe/CdSe type-II QDs by appropriated band engineering allows the TiO_2 CB position to be adjusted for pushing up the V_{oc}. Therefore, constructing type-II core/shell structured QDs is a promising way to develop panchromatic QD sensitizers for high-performance QDSCs. This work paves the way for further improving QDSCs performance based on advanced QD design, not just focusing on the light harvesting but on the effective interaction with the surrounding media.

MATERIALS AND METHODS

Chemicals. Cadmium oxide (CdO, 99.999%), selenium powder (99.99%, 100 mesh), octadecylamine (ODA, 97%), oleylamine (OAm, 95%), 1-octadecene (ODE, 90%), trioctylphosphine (TOP, 90%), and diethylzinc ($ZnEt_2$) were purchased from Aldrich Sigma. Tellurium powder (99.99%, 100 mesh) was purchased from Aladdin, China. Oleic acid (90%), and tetradecylphosphonic acid (TDPA, 98%) were obtained from Alfa Aesar. All chemicals were used as received without further treatment.

Synthesis and Water Solubilization of Initial Oil-Soluble ZnTe/CdSe Core/Shell QDs. ODA-capped oil-soluble ZnTe/CdSe core/shell QDs were prepared *via* a two-step procedure following a standard literature method.[36] First, 3.2 nm ZnTe core QDs were synthesized by the injection of Te and Zn precursor mixture solutions (TOP-Te and $ZnEt_2$, respectively) in ODA and ODE mixture media at 280 °C and growth for 3 min at 270 °C. The CdSe shell was then grown using the successive ion layer adsorption and reaction (SILAR) procedure. After the reaction mixture was cooled to 240 °C, equimolar amounts of Se and Cd precursor solutions (both 0.1 M) were injected alternately into the crude ZnTe QD reaction system at 10 min intervals, and 5.3 nm ZnTe/CdSe core/shell QDs were obtained after three cycles of SILAR procedure. The reaction mixture was dissolved in hexanes and then isolated and purified by centrifugation and decantation with the addition of acetone. CdSe QDs serving as reference with identical particle sizes of 5.3 nm were synthesized according to literature methods.[50] Absorption and photoluminescence (PL) emission spectra of QD dispersions were measured on a Shimadzu UV-3101 spectrophotometer and a fluorescence spectrophotometer (Cary Eclipse Varian), respectively. Transmission electron microscopy (TEM) measurements were performed on a JEOL JEM-2100 microscope.

The water solubilization of the as-prepared oil-soluble QDs and the access of MPA-capped water-soluble QDs were achieved by replacing the initial hydrophobic surfactants (ODA and/or TOP) with hydrophilic MPA at ambient atmosphere at room temperature according to literature methods.[37,51] The free MPA ligand in the QD aqueous solution was isolated by precipitating the QDs with addition of acetone. The supernatant was discarded, and the pellet was then redissolved in water for use in the next step.

Construction and Characterization of QDSCs. TiO_2 mesoporous film electrodes were prepared by successive screen printing of the transparent layer (9.0 ± 0.5 μm) with use of homemade P25 paste and a light-scattering/opaque layer (6.0 ± 0.5 μm) using 30 wt % 200−400 nm TiO_2 mixed with 70 wt % P25 paste over clean F:SnO_2 glass (FTO, 8 Ω/square) substrates.[38] Before the coating of TiO_2 paste, the FTO glass was first cleaned according to the standard procedure and then soaked into a 40 mM $TiCl_4$ aqueous solution and kept at 70 °C for 30 min followed by washing with water and ethanol. For immobilization of QDs on TiO_2 film electrodes, a drop of MPA-capped QDs aqueous solution (30 μL, with absorbance of 2.0 at 600 nm) was pipetted onto the TiO_2 film surface and kept for 2−4 h before being rinsed with water and ethanol sequentially. After completion of the deposition, the QD-sensitized TiO_2 photoanodes were coated with a thin layer of ZnS by immersion into $Zn(OAc)_2$ and Na_2S aqueous solutions (0.1 M for both) alternately for four cycles.

The Cu_2S/brass counter electrodes were obtained by immersing brass foil in HCl solution (1.0 M) at 70 °C for 10 min and then vulcanized by insertion into the polysulfide electrolyte solution for 10 min. The composition of the redox electrolyte solution is 2.0 M Na_2S, 2.0 M S, and 0.2 M KCl in distilled water. The solar cells were constructed by assembling the Cu_2S/brass counter electrode and QD-sensitized TiO_2 film electrode with a binder clip separated by a 50 μm thickness Scotch spacer. Polysulfide electrolyte solution was then filled inside the cell. For each QDSC studied, at least seven cells in parallel were constructed, and the average performance was evaluated.

Photovoltaic performances ($J-V$ curves) of QDSCs were measured using a Keithley 2400 source meter, and the illumination source was a 150 W AM 1.5G solar simulator (Oriel, Model No. 94022A). The intensity of the simulated solar light was calibrated to 100 mW cm^{-2} by standard silicon solar cell supported by NREL. The photoactive area of 0.233 cm^2 was defined by a black plastic circular mask. An incident photon-to-current conversion efficiency (IPCE) spectrum was obtained by a Keithley 2000 multimeter under illumination with a 300 W tungsten lamp with a Spectral Product DK240 monochromator. Electrochemical impedance spectroscopy (EIS) measurements were performed on an impedance analyzer (Zahner, Zennium) in the dark or under irradiation conditions supported by a white LED with intensity of 50 mW/cm^2 at different forward bias, applying a 20 mV AC sinusoidal signal over the constant applied bias with the frequency ranging from 1 MHz to 0.1 Hz. To verify the validity of EIS data, $J-V$ curves were recorded before and after each EIS measurement. Experimental results demonstrate that no significant variation in the photovoltaic parameters for ZnTe/CdSe based QDSCs was observed. Charge-extraction measurement were conducted on the same electrochemical workstation under the Charge Extraction module with 10 ms time-resolution. In the measurement, the studied cells are subject to the irradiation by an intensity-modulated (200−1200 W/m^2) white LED driven by a Zahner source supply under open circuit conditions. When a steady V_{oc} is reached at a specific illumination intensity, the light is switched off and the accumulated charge in the photoanode is collected by short circuiting the testing cell *via* a known resistor. The corresponding electron density can then be obtained by integration of the current trace.

TG Measurement. The TG measurement was carried out with a pump pulse wavelength of 450 nm and probe pulse wavelength of 775 nm under nitrogen atmosphere. The laser source is a titanium/sapphire laser (CPA-2010, Clark-MXR, Inc.) with a wavelength of 775 nm, repetition rate of 1000 Hz, and pulse

width of 150 fs. The light was divided into two parts. One part was used as the probe pulse; the other as the pump light to pump an optical parametric amplifier (TOAPS from Quantronix) to generate light pulses with wavelengths tunable from 290 nm to 3 μm. Typical laser pulse intensity used in this TG meaurement was 2.0 mW. The area of the laser beam was ~0.2 cm^2. All testing samples showed no apparent photodamage during the TG measurements. The principle of the improved TG method has been explained in detail in our previous reports.[47,48,52]

Conflict of Interest: The authors declare no competing financial interest.

Acknowledgment. We acknowledge the National Natural Science Foundation of China (Nos. 21421004, 91433106, and 21175043), the Science and Technology Commission of Shanghai Municipality (11JC1403100 and 12NM0504101), the Fundamental Research Funds for the Central Universities in China, the CREST program of Japan Science and Technology Agency (JST), and Grant in Aid for Scientific Research (No. 26286013) from the Ministry of Education, Sports, Science and Technology of the Japanese Government for financial support.

Supporting Information Available: Detailed synthetic procedure; optical and TEM characterization of ZnTe/CdSe QDs. Optical characterization of CdSe QDs and CdTe/CdSe QDs. *J*−*V* curves and photovoltaic parameters of ZnTe/CdSe-, CdSe-, and CdTe/CdSe-based cell devices (each group has seven devices in parallel). Certified report for photovoltaic performance of ZnTe/CdSe cell. Nyquist curves under dark and illumination conditions on different bias voltages for ZnTe/CdSe- and CdTe/CdSe-based cells. The dependence of recombination resistance on applied voltage under dark and illumination for ZnTe/CdSe and CdTe/CdSe-based cells. This material is available free of charge *via* the Internet at http://pubs.acs.org.

REFERENCES AND NOTES

1. Lohse, S. E.; Murphy, C. J. Applications of Colloidal Inorganic Nanoparticles: From Medicine to Energy. *J. Am. Chem. Soc.* **2012**, *134*, 15607–15620.
2. Semonin, O. E.; Luther, J. M.; Choi, S.; Chen, H. Y.; Gao, J. B.; Nozik, A. J.; Beard, M. C. Peak External Photocurrent Quantum Efficiency Exceeding 100% *via* MEG in a Quantum Dot Solar Cell. *Science* **2011**, *334*, 1530–1533.
3. Nozik, A. J.; Beard, M. C.; Luther, J. M.; Law, M.; Ellingson, R. J.; Johnson, J. C. Semiconductor Quantum Dots and Quantum Dot Arrays and Applications of Multiple Exciton Generation to Third-Generation Photovoltaic Solar Cells. *Chem. Rev.* **2010**, *110*, 6873–6890.
4. Kramer, I. J.; Sargent, E. H. The Architecture of Colloidal Quantum Dot Solar Cells: Materials to Devices. *Chem. Rev.* **2014**, *114*, 863–882.
5. Sambur, J. B.; Novet, T.; Parkinson, B. A. Multiple Exciton Collection in a Sensitized Photovoltaic System. *Science* **2010**, *330*, 63–66.
6. Kershaw, S. V.; Susha, A. S.; Rogach, A. L. Narrow Bandgap Colloidal Metal Chalcogenide Quantum Dots: Synthetic Methods, Heterostructures, Assemblies, Electronic and Infrared Optical Properties. *Chem. Soc. Rev.* **2013**, *42*, 3033–3087.
7. Pan, Z. X.; Mora-Seró, I.; Shen, Q.; Zhang, H.; Li, Y.; Zhao, K.; Wang, J.; Zhong, X. H.; Bisquert, J. High-Efficiency "Green" Quantum Dot Solar Cells. *J. Am. Chem. Soc.* **2014**, *136*, 9203–9210.
8. Wang, J.; Mora-Sero, I.; Pan, Z. X.; Zhao, K.; Zhang, H.; Feng, Y.; Yang, G.; Zhong, X. H.; Bisquert, J. Core/Shell Colloidal Quantum Dot Exciplex States for the Development of Highly Efficient Quantum-Dot-Sensitized Solar Cells. *J. Am. Chem. Soc.* **2013**, *135*, 15913–15922.
9. Pan, Z.; Zhao, K.; Wang, J.; Zhang, H.; Feng, Y. Y.; Zhong, X. H. Near Infrared Absorption of $CdSe_xTe_{1-x}$ Alloyed Quantum Dot Sensitized Solar Cells with More than 6% Efficiency and High Stability. *ACS Nano* **2013**, *7*, 5215–5222.
10. Yan, K. Y.; Zhang, L. X.; Qiu, J. H.; Qiu, Y. C.; Zhu, Z. L.; Wang, J. N.; Yang, S. H. A Quasi-Quantum Well Sensitized Solar Cell with Accelerated Charge Separation and Collection. *J. Am. Chem. Soc.* **2013**, *135*, 9531–9539.
11. Luo, J. H.; Wei, H. Y.; Huang, Q. L.; Hu, X.; Zhao, H. F.; Yu, R. C.; Li, D. M.; Luo, Y. H.; Meng, Q. B. Highly Efficient Core−Shell $CuInS_2$−Mn Doped CdS Quantum Dot Sensitized Solar Cells. *Chem. Commun.* **2013**, *49*, 3881–3883.
12. McDaniel, H.; Fuke, N.; Makarov, N. S.; Pietryga, J. M.; Klimov, V. I. An Integrated Approach to Realizing High-Performance Liquid-Junction Quantum Dot Sensitized Solar Cells. *Nat. Commun.* **2013**, *4*, 2887.
13. Yu, X. Y.; Liao, J. Y.; Qiu, K. Q.; Kuang, D. B.; Su, C. Y. Dynamic Study of Highly Efficient CdS/CdSe Quantum Dot-Sensitized Solar Cells Fabricated by Electrodeposition. *ACS Nano* **2011**, *5*, 9494–9500.
14. Santra, P. K.; Kamat, P. V. Mn-Doped Quantum Dot Sensitized Solar Cells: A Strategy to Boost Efficiency over 5%. *J. Am. Chem. Soc.* **2012**, *134*, 2508–2511.
15. Hodes, G. Comparison of Dye- and Semiconductor-Sensitized Porous Nanocrystalline Liquid Junction Solar Cells. *J. Phys. Chem. C* **2008**, *112*, 17778–17787.
16. Kamat, P. V. Quantum Dot Solar Cells. Semiconductor Nanocrystals as Light Harvesters. *J. Phys. Chem. C* **2008**, *112*, 18737–18753.
17. Mora-Seró, I.; Gimenez, S.; Fabregat-Santiago, F.; Gomez, R.; Shen, Q.; Toyoda, T.; Bisquert, J. Recombination in Quantum Dot Sensitized Solar Cells. *Acc. Chem. Res.* **2009**, *42*, 1848–1857.
18. Ruhle, S.; Shalom, M.; Zaban, A. Quantum-Dot-Sensitized Solar Cells. *ChemPhysChem* **2010**, *11*, 2290–2304.
19. Yaacobi-Gross, N.; Garphunkin, N.; Solomeshch, O.; Vaneski, A.; Susha, A. S.; Rogach, A. L.; Tessler, N. Combining Ligand-Induced Quantum-Confined Stark Effect with Type II Heterojunction Bilayer Structure in CdTe and CdSe Nanocrystal-Based Solar Cells. *ACS Nano* **2012**, *6*, 3128–3133.
20. Kamat, P. V. Boosting the Efficiency of Quantum Dot Sensitized Solar Cells through Modulation of Interfacial Charge Transfer. *Acc. Chem. Res.* **2012**, *45*, 1906–1915.
21. Wang, H.; Luan, C.; Xu, X.; Kershaw, S. V.; Rogach, A. L. In Situ versus ex Situ Assembly of Aqueous-Based Thioacid Capped CdSe Nanocrystals within Mesoporous TiO_2 Films for Quantum Dot Sensitized Solar Cells. *J. Phys. Chem. C* **2012**, *116*, 484–489.
22. Kamat, P. V. Quantum Dot Solar Cells. The Next Big Thing in Photovoltaics. *J. Phys. Chem. Lett.* **2013**, *4*, 908–918.
23. Hetsch, F.; Xu, X.; Wang, H.; Kershaw, S. V.; Rogach, A. L. Semiconductor Nanocrystal Quantum Dots as Solar Cell Components and Photosensitizers: Material, Charge Transfer, and Separation Aspects of Some Device Topologies. *J. Phys. Chem. Lett.* **2011**, *2*, 1879–1887.
24. Kim, S.; Fisher, B.; Eisler, H. J.; Bawendi, M. Type-II Quantum Dots: CdTe/CdSe (Core/Shell) and CdSe/ZnTe (Core/Shell) Heterostructures. *J. Am. Chem. Soc.* **2003**, *125*, 11466–11467.
25. Zhong, H. Z.; Zhou, Y.; Yang, Y.; Yang, C. H.; Li, Y. F. Synthesis of Type II CdTe-CdSe Nanocrystal Heterostructured Multiple-Branched Rods and Their Photovoltaic Applications. *J. Phys. Chem. C* **2007**, *111*, 6538–6543.
26. Scholes, G. D.; Jones, M.; Kumar, S. Energetics of Photoinduced Electron-Transfer Reactions Decided by Quantum Confinement. *J. Phys. Chem. C* **2007**, *111*, 13777–13785.
27. Bang, J.; Park, J.; Lee, J. H.; Won, N.; Nam, J.; Lim, J.; Chang, B. Y.; Lee, H. J.; Chon, B.; Shin, J.; et al. ZnTe/ZnSe (Core/Shell) Type-II Quantum Dots: Their Optical and Photovoltaic Properties. *Chem. Mater.* **2010**, *22*, 233–240.
28. Zhu, H.; Song, N.; Lian, T. Wave Function Engineering for Ultrafast Charge Separation and Slow Charge Recombination in Type II Core/Shell Quantum Dots. *J. Am. Chem. Soc.* **2011**, *133*, 8762–8771.
29. Lo, S. S.; Mirkovic, T.; Chuang, C. H.; Burda, C.; Scholes, G. D. Emergent Properties Resulting from Type-II Band Alignment in Semiconductor Nanoheterostructures. *Adv. Mater.* **2011**, *23*, 180–197.
30. Ning, Z. J.; Tian, H. N.; Yuan, C. Z.; Fu, Y.; Qin, H. Y.; Sun, L. C.; Agren, H. Solar Cells Sensitized with Type-II ZnSe-CdS

Core/Shell Colloidal Quantum Dots. *Chem. Commun.* **2011**, *47*, 1536–1538.
31. Itzhakov, S.; Shen, H.; Buhbut, S.; Lin, H.; Oron, D. Type-II Quantum-Dot-Sensitized Solar Cell Spanning the Visible and Near-Infrared Spectrum. *J. Phys. Chem. C* **2013**, *117*, 22203–22210.
32. Buhbut, S.; Itzhakov, S.; Hod, I.; Oron, D.; Zaban, A. Photo-Induced Dipoles: A New Method to Convert Photons into Photovoltage in Quantum Dot Sensitized Solar Cells. *Nano Lett.* **2013**, *13*, 4456–4461.
33. Kazes, M.; Buhbut, S.; Itzhakov, S.; Lahad, O.; Zaban, A.; Oron, D. Photophysics of Voltage Increase by Photo-induced Dipole Layers in Sensitized Solar Cells. *J. Phys. Chem. Lett.* **2014**, *5*, 2717–2722.
34. Wei, S.-H.; Zunger, A. Calculated Natural Band Offsets of All II–VI and III–V Semiconductors: Chemical Trends and the Role of Cation *d* Orbitals. *Appl. Phys. Lett.* **1998**, *72*, 2011.
35. Choi, Y. C.; Lee, D. U.; Noh, J. H.; Kim, E. K.; Seok, S. I. Highly Improved Sb_2S_3 Sensitized-Inorganic-Organic Heterojunction Solar Cells and Quantification of Traps by Deep-Level Transient Spectroscopy. *Adv. Funct. Mater.* **2014**, *24*, 3587–3592.
36. Xie, R. G.; Zhong, X. H.; Basche, T. Synthesis, Characterization, and Spectroscopy of Type-II Core/Shell Semiconductor Nanocrystals with ZnTe Cores. *Adv. Mater.* **2005**, *17*, 2741–2745.
37. Zhang, H.; Cheng, K.; Hou, Y.; Fang, Z.; Pan, Z. X.; Wu, W. J.; Hua, J. L.; Zhong, X. H. Efficient CdSe Quantum Dot-Sensitized Solar Cells Prepared by a Postsynthesis Assembly Approach. *Chem. Commun.* **2012**, *48*, 11235–11237.
38. Du, Z. L.; Zhang, H.; Bao, H. L.; Zhong, X. H. Optimization of TiO_2 Photoanode Films for Highly Efficient Quantum Dot-Sensitized Solar Cells. *J. Mater. Chem. A* **2014**, *2*, 13033–13040.
39. Ning, Z. J.; Zhitomirsky, D.; Adinolfi, V.; Sutherland, B.; Xu, J.; Voznyy, O.; Maraghechi, P.; Lan, X.; Hoogland, S.; Ren, Y. et al. Graded Doping for Enhanced Colloidal Quantum Dot Photovoltaics. *Adv. Mater.* **2013**, *25*, 1719–1723.
40. Chuang, C. M.; Brown, P. R.; Bulovic, V.; Bawendi, M. G. Improved Performance and Stability in Quantum Dot Solar Cells through Band Alignment Engineering. *Nat. Mater.* **2014**, *13*, 796–801.
41. Ning, Z. J.; Voznyy, O.; Pan, J.; Hoogland, S.; Adinolfi, V.; Xu, J. X.; Li, M.; Kirmani, A. R.; Sun, J.-P.; Minor, J.; et al. Air-Stable n-Type Colloidal Quantum Dot Solids. *Nat. Mater.* **2014**, *13*, 822–828.
42. Hossain, M. A.; Jennings, J. R.; Shen, C.; Pan, J. H.; Koh, Z. Y.; Mathews, N.; Wang, Q. CdSe-Sensitized Mesoscopic TiO_2 Solar Cells Exhibiting >5% Efficiency: Redundancy of CdS Buffer Layer. *J. Mater. Chem.* **2012**, *22*, 16235–16242.
43. González-Pedro, V.; Xu, X.; Mora-Seró, I.; Bisquert, J. Modeling High-Efficiency Quantum Dot Sensitized Solar Cells. *ACS Nano* **2010**, *4*, 5783–5790.
44. Fabregat-Santiago, F.; Garcia-Belmonte, G.; Mora-Seró, I.; Bisquert, J. Characterization of Nanostructured Hybrid and Organic Solar Cells by Impedance Spectroscopy. *Phys. Chem. Chem. Phys.* **2011**, *13*, 9083–9118.
45. Raga, S. R.; Barea, E. M.; Fabregat-Santiago, F. Analysis of the Origin of Open Circuit Voltage in Dye Solar Cells. *J. Phys. Chem. Lett.* **2012**, *3*, 1629–1634.
46. Shen, Q.; Yanai, M.; Katayama, K.; Sawada, T.; Toyoda, T. Optical Absorption, Photosensitization, and Ultrafast Carrier Dynamic Investigations of CdSe Quantum Dots Grafted onto Nanostructured SnO_2 Electrode and Fluorine-Doped Tin Oxide (FTO) Glass. *Chem. Phys. Lett.* **2007**, *442*, 89–96.
47. Gonzalez-Pedro, V.; Sima, C.; Marzari, G.; Boix, P. P.; Gimenez, S.; Shen, Q.; Dittrich, T.; Mora-Seró, I. High Performance PbS Quantum Dot Sensitized Solar Cells Exceeding 4% Efficiency: the Role of Metal Precursors in the Electron Injection and Charge Separation. *Phys. Chem. Chem. Phys.* **2013**, *15*, 13835–13843.
48. Yang, J. W.; Oshima, T.; Oshima, W.; Pan, Z. X.; Zhong, X. H.; Shen, Q. Influence of Linker Molecules on Interfacial Electron Transfer and Photovoltaic Performance of Quantum Dot Sensitized Solar Cells. *J. Mater. Chem. A* **2014**, *2*, 20882–20888.
49. Kongkanand, A.; Tvrdy, K.; Takechi, K.; Kuno, M.; Kamat, P. V. Quantum Dot Solar Cells. Tuning Photoresponse through Size and Shape Control of CdSe–TiO_2 Architecture. *J. Am. Chem. Soc.* **2008**, *130*, 4007–4015.
50. Zhong, X. H.; Feng, Y. Y.; Zhang, Y. L. Facile and Reproducible Synthesis of Red-Emitting CdSe Nanocrystals in Amine with Long-Term Fixation of Particle Size and Size Distribution. *J. Phys. Chem. C* **2007**, *111*, 526–531.
51. Liu, L.; Zhong, X. H. A General and Reversible Phase Transfer Strategy Enabling Nucleotides Modified High-Quality Water-Soluble Nanocrystals. *Chem. Commun.* **2012**, *48*, 5718–5720.
52. Katayama, K.; Yamaguchi, M.; Sawada, T. Lens-Free Heterodyne Detection for Transient Grating Experiments. *Appl. Phys. Lett.* **2003**, *82*, 2775–2777.